Secondary-Phase-Assisted Grain Boundary Migration in $CuInSe_2$

Chen Li,[1,*,†] Ekin Simsek Sanli,[1] Daniel Barragan-Yani,[2] Helena Stange,[3] Marc-Daniel Heinemann,[4] Dieter Greiner,[4] Wilfried Sigle,[1] Roland Mainz,[4] Karsten Albe,[2] Daniel Abou-Ras,[4] and Peter A. van Aken[1]

[1]*Stuttgart Center for Electron Microscopy, Max Planck Institute for Solid State Research, 70569 Stuttgart, Germany*
[2]*Institute of Materials Science, Technical University Darmstadt, 64287 Darmstadt, Germany*
[3]*Institute of Materials Science and Technology, Technical University Berlin, 10587 Berlin, Germany*
[4]*Helmholtz-Zentrum Berlin für Materialien und Energie GmbH, 14109 Berlin, Germany*

(Received 19 September 2019; accepted 8 January 2020; published 5 March 2020)

Significant structural evolution occurs during the deposition of $CuInSe_2$ solar materials when the Cu content increases. We use *in situ* heating in a scanning transmission electron microscope to directly observe how grain boundaries migrate during heating, causing nondefected grains to consume highly defected grains. Cu substitutes for In in the near grain boundary regions, turning them into a Cu-Se phase topotactic with the $CuInSe_2$ grain interiors. Together with density functional theory and molecular dynamics calculations, we reveal how this Cu-Se phase makes the grain boundaries highly mobile.

DOI: 10.1103/PhysRevLett.124.095702

Thin-film solar cells with $Cu(In,Ga)Se_2$ (CIGS) absorber layers have reached conversion efficiencies of up to 23.35% [1–6]. For fabricating high-performance CIGS absorber layers, a three-stage coevaporation process has been established [7]. In the second stage of this process, Cu-Se is coevaporated on a $(In,Ga)_2Se_3$ precursor forming a CIGS layer, during which the $[Cu]/([In]+[Ga])$ ratio changes from <1 to >1, referred to as the "Cu-poor to Cu-rich transition" (Supplemental Material [8], Fig. S01). Significant structural changes occur during this transition, including an increase in the average grain size [16–19], a decrease in the stacking fault density [19–21], compositional changes at the grain boundaries (GBs) [22], phase transitions [23], as well as stress relaxation [17,19]. In order to achieve a fundamental understanding of the structure evolution, structural information during growth down to the atomic scale is essential, which has so far remained lacking.

In the present study, CIS was chosen as an initial system in order to exclude the complicating issue of the Ga/In gradient change in the CIGS system. We monitored both structural and compositional evolutions in detail during the Cu-poor to Cu-rich transition in CIS thin films by performing *in situ* heating inside a scanning transmission electron microscope (STEM). The results show that grains with high-density planar defects tend to be consumed by grains without apparent planar defects. Furthermore, elemental mapping revealed that a Cu-Se secondary phase formed adjacent to the GBs, which was shown to support high ionic conductivity by density functional theory (DFT) calculations. Combining all these results leads to an overall picture and fundamental understanding of how Cu and In diffusion at GBs assists the GB migration and grain growth. Such a secondary-phase-assisted GB migration mechanism not only can apply to similar systems such as $CuInS_2$ with Cu or Ag diffusion [24,25], but might also be intentionally induced in other polycrystalline materials such as ceramics [26,27] or semiconductors [28,29] developing new methods of growth leading to defect-free materials.

A Cu-poor CIS layer was deposited on glass via a coevaporation process. An additional Cu-Se layer was deposited on this CIS layer at a low temperature of 150 °C to impede the diffusion between the two layers, until an integral Cu-rich composition was reached. Then a focused ion beam was used to prepare specimens for STEM. Time-series STEM images and electron energy-loss spectroscopy (EELS) elemental maps recorded during *in situ* heating were converted into movies (Supplemental Material [8–15]). Annular dark-field (ADF) imaging was used, in which the intensity is roughly proportional to the square of the atomic number Z, so-called Z-contrast imaging [30]. The VASP package [31] was used to carry out DFT calculations. The diffusion processes were simulated via *ab initio* molecular dynamics (MD) calculations. For more details see the Supplemental Material [8].

Figure 1 (from movie 1 in the Supplemental Material [8]) shows typical microstructural changes that occur during *in situ* heating. The planar defects are visible as parallel lines in the CIS grains. A comparison with the structure before and after being heated up to 450 °C shows that the CIS grains with high-density planar defects tend to be consumed by the grains without apparent planar defects.

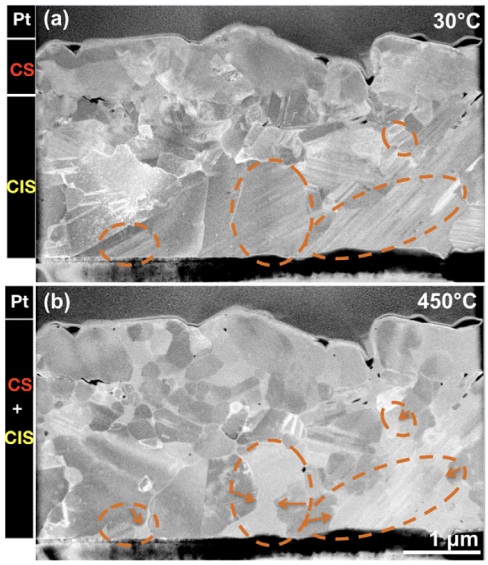

FIG. 1. Structure (a) before and (b) after *in situ* heating in STEM (extracted from movie 1 in the Supplemental Material [8]) shows that the CIS grains with high-density planar defects (marked by orange dashed ovals) tend to be consumed by the grains without planar defects. GBs migration directions are marked by orange arrows.

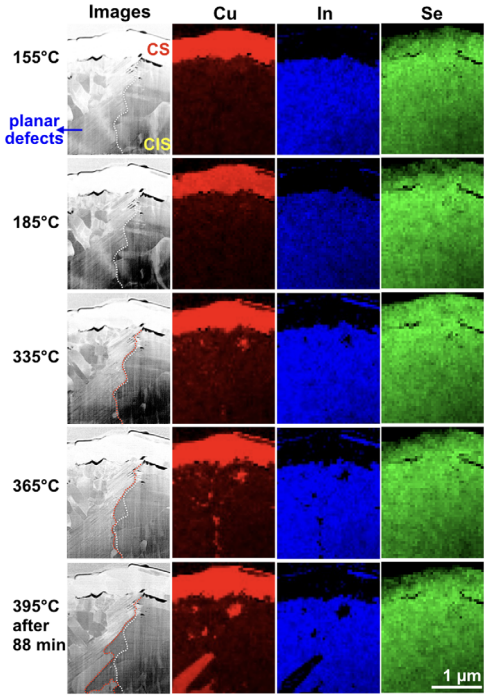

FIG. 2. Simultaneous STEM imaging and EELS elemental mapping during *in situ* heating of a CS/CIS specimen (extracted from movies 3–6). In the contrast-enhanced images, the white dashed lines mark the original GB position, while the red dashed lines mark its current position. The grain with high-density planar defects became smaller during heating, while the grain on its right side without planar defects grew larger. Cu accumulated and In depleted at the migrating GB between these two grains.

This is consistent with results obtained by *in situ* XRD [32]. Always, the GB migration directions are towards the grains containing high-density planar defects.

We also performed a comparison experiment on a similar CIS layer, but without the excess CS capping layer (Supplemental Material, Fig. S02 and movie 2). No GB migration was observed, and the high-density planar defects within the CIS grains still remained, showing that below 450 °C an excess CS layer is essential for the GB migration.

To understand how the excess CS layer affects the grain growth, we performed simultaneous STEM imaging (movie 3) and EELS elemental mapping (movies 4–6) during *in situ* heating of the CS/CIS specimen. Cu diffused from the CS capping layer towards the CIS layer, while In diffused from CIS towards the CS layer. In contrast, the Se distribution did not exhibit any substantial change during the entire process.

Various phenomena were observed at different temperatures, and a selection of important compositional changes are shown in Fig. 2.

(i) At 155 °C, the Cu concentration in the CIS layer increased gradually.

(ii) At 185 °C, In started to segregate to the top surface of the CS capping layer, forming new CIS islands at the top surface of the CS layer.

(iii) At 245 °C, Cu started to become enriched along the CIS GBs.

(iv) At 335 °C, GBs started to migrate slowly.

(v) At 365 °C, GB migration became more obvious: the grains with high-density planar defects were consumed by the grains without planar defects. Cu enrichment and In depletion were observed at the migrating GB.

(vi) At 395 °C, Cu replaced some In transforming some CIS grains into CS grains (Supplemental Material, Fig. S03 [33]).

(vii) After heating up to 450 °C, 10.5% of the CIS layer has transformed to the $Cu_{2-x}Se$ phase. 22.0% of the CS layer has transformed to the CIS phase.

Higher-resolution EELS maps consistently show Cu enrichment and In depletion at GBs, while the Se concentration remains almost unchanged, as shown in Fig. 3(a). Such Cu-rich and In-poor CIS GBs have also been reported in CIGS and CIS interrupted at early growth stages [34]. More detailed investigations show that the chemical variations are, however, not sharply localized at the GB planes as reported in completed CIGS thin films [35] or other thin film solar materials [36,37], but are spread over 10–20 nm from the GB planes (Supplemental Material, Fig. S04).

Atomic-resolution imaging at such Cu-rich and In-poor GBs shows a gradual phase transition [Fig. 3(b)] from a chalcopyrite $CuInSe_2$ phase [Fig. 3(d)] inside the CIS grain towards an antifluorite (Fm-$3m$) $Cu_{2-x}Se$ phase [Fig. 3(c)] near GBs. The antifluorite $Cu_{2-x}Se$ phase is known as the high-temperature phase of this material [38,39]. The possibility of phases overlapping or crystal bending can

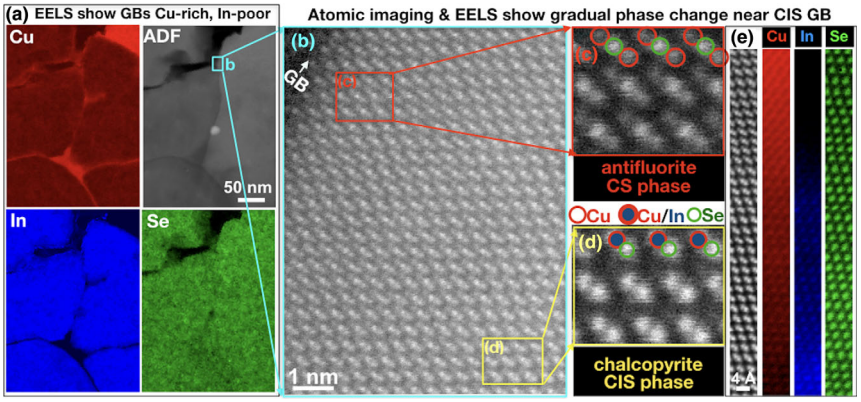

FIG. 3. (a) EELS mapping shows Cu enrichment and In depletion at all GBs. (b)–(d) Atomic-resolution Z-contrast images show a gradual phase transition from (d) a chalcopyrite phase $CuInSe_2$ inside the grain towards (c) an antifluorite (Fm-$3m$) phase $Cu_{2-x}Se$ near the GB. (e) EELS elemental maps confirm this gradual phase change: Se atoms stay in their lattice, while Cu and In interdiffuse.

be excluded because atomic-resolution EELS mapping [Fig. 3(e)] confirms this gradual phase change: Se atoms remain on their lattice sites, while Cu and In interdiffuse. The corresponding concentration maps for Fig. 3(e) are shown in Supplemental Material, Fig. S05, demonstrating a gradual composition transition from 25% Cu, 23% In, and 52% Se in the CIS phase to 59% Cu, 6% In, and 35% Se towards the CS phase. The structure of this intermediate phase can be considered as an antifluorite (Fm-$3m$) $Cu_{2-x}Se$ phase with In atoms sitting on some Cu sites (Fig. S06). More towards the GBs, the In concentration becomes zero at the Cu/In sites and the intermediate CIS phase becomes antifluorite CS.

In the past, a topotactic reaction of CS and CIS with a continuous Se lattice was suggested for the growth of CIS crystals from a Cu-Se liquid on the surface of CIS, with an intermediate solid $Cu_{2-x}Se$ phase [40,41]. Occasionally, small platelets with $Cu_{2-x}Se$ phases were found at GBs in Cu-poor CIGS [42]. Our results show that such topotactic transitions between CIS and $Cu_{2-x}Se$ phases commonly exist near the CIS GBs when sufficient Cu diffuses into GBs.

In order to understand the Cu and In diffusion, DFT calculations were carried out to obtain the formation energies of intrinsic defects in the antifluorite phase Cu_2Se. DFT results (Supplemental Material, Fig. S07) demonstrate that the formation energy of a Cu vacancy (V_{Cu}) is negative (< -0.2 eV), implying that Cu vacancies easily form leading to the observed $Cu_{2-x}Se$ configuration. Furthermore, it is found that the formation energy of an In_{Cu} antisite defect (2–2.9 eV) is low enough for some In atoms to occupy Cu sites in the antifluorite $Cu_{2-x}Se$ lattice forming the observed intermediate CIS phase.

Furthermore, the nudged elastic band (NEB) method was used to calculate the diffusion energy barriers for the relevant defects (Supplemental Material, Fig. S07). The diffusion barrier for Cu to jump from an interstitial site (Cu_i) to another Cu_i is about 1 eV, while from one V_{Cu} to

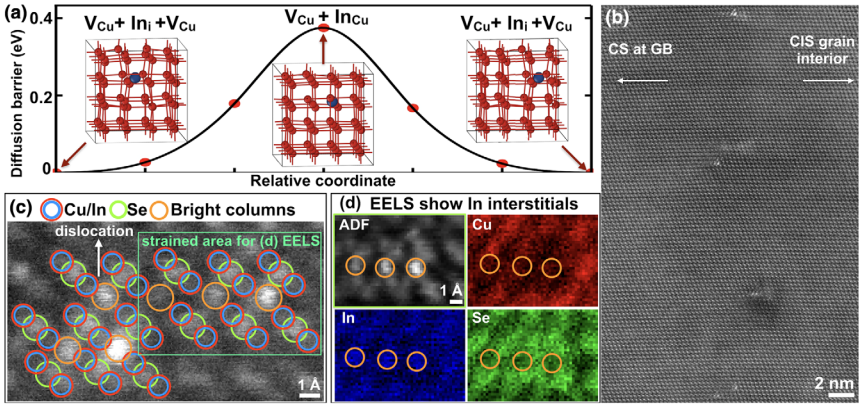

FIG. 4. (a) DFT calculations show that in the presence of V_{Cu}, the diffusion barrier for an In atom (blue ball) to move from one interstitial to another interstitial position is only ~0.38 eV. The red balls show the Cu sublattice. (b) STEM Z-contrast imaging shows bright contrast at dislocations along a small-angle GB at the intermediate CIS phase. (c) Columns with bright contrast appear between the normal Cu/In and Se sites, both at and near the dislocation. (d) EELS mapping shows the interstitial columns are In, and Cu depletion occurs in the area, supporting the DFT results of easy formation of $V_{Cu} + In_i + V_{Cu}$ clusters.

another V_{Cu} is much lower, below 0.2 eV. Therefore, vacancy-assisted Cu diffusion can occur easily in this CS structure, which is consistent with previous reports that refer to the $Cu_{2-x}Se$ phase as a superionic conductor [38,39].

Next, the diffusion barrier for In in CS was calculated. Moving an In_{Cu} from one Cu site to another Cu site without the presence of Cu vacancies would involve the formation of both In and Cu interstitials, which is energetically unfavorable. Interestingly, as soon as there is a V_{Cu} next to the In_{Cu}, the structure relaxes into a configuration in which the In atom is located in an interstitial site becoming In_i, and is surrounded by two V_{Cu} sites ($V_{Cu} + In_i + V_{Cu}$ cluster), as shown in the initial and final structure in Fig. 4(a). In such a configuration the diffusion barrier of In_i is only ~0.38 eV, showing that In exhibits fast diffusion in $Cu_{2-x}Se$ with the assistance of nearby V_{Cu}. Such a vacancy-assisted ion diffusion mechanism is similar to the one suggested for Y diffusion in Fe [43].

Since the NEB method only calculates the energy barriers for single jumps, we also carried out *ab initio* MD calculations to simulate a continuous In diffusion process at 700 K (Supplemental Material, Fig. S08). The results further indicate that In prefers to jump from interstitial to interstitial site with two neighboring V_{Cu}, suggesting a V_{Cu}-assisted In diffusion mechanism.

Using STEM we indeed detected the In interstitials at strained areas near CIS GBs. As shown in Fig. 4(b), columns with bright contrast are found at periodic dislocations along a small-angle boundary near CIS GBs. *Z*-contrast imaging in Fig. 4(c) shows that columns with bright contrast are located at atomic sites in between Cu/In sites and Se sites. This observation applies for the dislocations and the strained area around them. For the latter case, the bright columns can be interpreted as accumulations of interstitial atoms. Atomic-resolution EELS elemental mapping in Fig. 4(d) shows In enrichment at the bright interstitial columns and Cu depletion at and near these sites. Se atomic positions are hardly affected. A spectrum image of a larger area containing a cluster of interstitials confirms this finding [Supplemental Material, Fig. S09(a)]. In enrichment and Cu depletion were also observed for the bright columns at the dislocation cores [Supplemental Material, Fig. S09(b)]. The bright contrast at the In columns comes from the high atomic number (49) of In compared with Cu (29) and Se (34), and likely also from the lattice strain.

The discovery of In interstitials with nearby Cu deficiency strongly supports the results of the DFT calculations, which show that the formation of $V_{Cu} + In_i + V_{Cu}$ clusters is energetically favorable. The situation in dislocation cores is more complicated as the atomic configuration with line defects is different from the perfect crystal. However, the existence of In columns in between Cu/In sites and Se sites with nearby Cu deficiency, might also happen because of the easy formation of $V_{Cu} + In_i + V_{Cu}$ clusters. Additionally, segregation of In atoms with coinciding Cu depletion was also found at random GBs, as shown in Figs. S10–S11 in the Supplemental Material. These results indicate that both the dislocations and GBs provide extra diffusion routes for In atoms, besides that through interstitials suggested by the MD simulation.

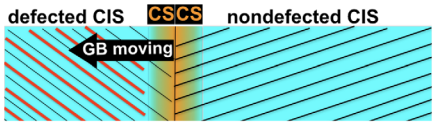

FIG. 5. Sketch showing the GB migration mechanism.

These results provide a comprehensive picture of how Cu-In diffusion assists GB migration in CIS (Fig. 5). The key is the formation of the secondary CS phase at the GBs. In the CS phase, Cu is highly mobile, and In can easily diffuse through interstitials with the assistance of surrounding Cu vacancies. The fast diffusion of Cu and In atoms in the CS phase also explains why In already diffused through the capping CS layer and replaced the surface Cu at temperatures below 185 °C. For the case of CIS GBs without an extra CS phase, all Cu, In, and Se atoms need to rearrange in order to migrate the CIS|CIS GBs, a process which requires a high enthalpy. However, when extra CS phases form at the CIS GBs, the GB geometry becomes CIS-CS|CS-CIS, and the CS phase at each side of the GB exhibits an atomic lattice topotactic with that of its adjacent CIS grain interior. Since both Cu and In can diffuse easily in the CS phase, the only energetically demanding factor for the GB migration is that of rearranging the Se lattice at the CS|CS boundary. Hence, the CIS-CS|CS-CIS GBs are far more mobile than the original CIS|CIS GBs.

Furthermore, the fact that the mobile GBs tend to migrate towards the defected CIS grains can be explained by the energy saved by removing lattice defects [32]. The reduction of the lattice defects increases the quality of the CIS absorber layers (likely also for CIGS), which explains why the Cu-poor to Cu-rich transition in the second stage is essential for device functionality. During the third stage of the three-stage growth process, the ratio of Cu/In decreases, and the CS secondary phase at the GBs might transform back to the CIS or CIGS phases. Nevertheless, such CS secondary phases are occasionally found at the GBs of bulk CIGS after a full three-stage growth [42], consistent with the present observation.

To summarize, using *in situ* heating in STEM, we directly monitored the structure evolution in CIS during a Cu-poor to Cu-rich transition. GBs migrate from nondefected CIS grains towards the highly defected grains. Cu-In diffusion transforms the nanometer-sized regions near the GBs into an antifluorite Cu_2Se phase, which exhibits a lattice topotactic with that of the CIS grain interiors. Theoretical calculations show that Cu and In are highly mobile in this CS phase, greatly enhancing the GB

mobility. These insights improve our understanding of the growth of CIS and CIGS solar materials, and might also reveal a general mechanism of GB migration and defect annihilation for a wide range of solid-state materials.

The research was financed in part by the Helmholtz Virtual Institute "Microstructure Control for Thin- Film Solar Cells" (VH-VI–520) project. This work has received additional funding from the European Union's Horizon 2020 research and innovation programme under Grant agreement No. 823717—ESTEEM3. E. S. S. thanks B. Fenk for the FIB sample preparation. C. L. thanks the Max Planck Society for the financial support and K. Hahn, Y. Wang, J. Deuschle, M. Kelsch, and U. Salzberger for technical support.

*chen.li@uantwerpen.be
lichen0320@gmail.com
†Present address: EMAT, University Antwerp, 2020 Antwerp, Belgium.

[1] T. Kato, J.-L. Wu, Y. Hirai, H. Sugimoto, and V. Bermudez, IEEE J. Photovoltaics **9**, 325 (2019).
[2] http://www.solar-frontier.com/eng/news/2019/0117_press.html.
[3] E. Gomibia, F. Leccabue, G. Salviati, and D. Seuret, J. Cryst. Growth **65**, 270 (1983).
[4] R. Janam and O. N. Srivastava, Solar Energy Mater. **19**, 395 (1989).
[5] D. S. Albin, G. D. Mooney, A. Duda, J. Tuttle, R. Matson, and R. Noufi, Sol. Cells **30**, 47 (1991).
[6] R. J. Gupta, D. Bhattacharya, and O. N. Srivastava, J. Cryst. Growth **87**, 151 (1988).
[7] A. M. Gabor, J. R. Tuttle, D. S. Albin, M. A. Contreras, R. Noufi, and A. M. Hermann, Appl. Phys. Lett. **65**, 198 (1994).
[8] See Supplemental Material at http://link.aps.org/supplemental/10.1103/PhysRevLett.124.095702 for additional details of the materials growth, sample preparation, electron microscopy, density functional and molecular dynamics calculations, as well as six movies showing the structural and compositional change during the *in situ* growth, which includes Refs. [9–15].
[9] M. Watanabe, E. Okunishi, and K. Ishizuka, Microsc. Anal. **23**, 5 (2009).
[10] G. Kresse and D. Joubert, Phys. Rev. B **59**, 1758 (1999).
[11] C. Adamo and V. Barone, J. Chem. Phys. **110**, 6158 (1999).
[12] J. P. Perdew, M. Ernzerhof, and K. Burke, J. Chem. Phys. **105**, 9982 (1996).
[13] J. P. Perdew, K. Burke, and M. Ernzerhof, Phys. Rev. Lett. **77**, 3865 (1996).
[14] G. Mills and H. Jónsson, Phys. Rev. Lett. **72**, 1124 (1994).
[15] A. Stukowski, Model. Simul. Mater. Sci. Eng. **18**, 015012 (2010).
[16] N. Barreau, T. Painchaud, F. Couzinié-Devy, L. Arzel, and J. Kessler, Acta Mater. **58**, 5572 (2010).
[17] R. Mainz, H. Rodriguez-Alvarez, M. Klaus, D. Thomas, J. Lauche, A. Weber, M.-D. Heinemann, S. Brunken, D. Greiner, C. A. Kaufmann, T. Unold, H. W. Schock, and C. Genzel, Phys. Rev. B **92**, 155310 (2015).
[18] R. Caballero, C. A. Kaufmann, V. Efimova, T. Rissom, V. Hoffmann, and H. W. Schock, Prog. Photovoltaics Res. Appl. **21**, 30 (2013).
[19] H. Stange, S. Brunken, D. Greiner, M.-D. Heinemann, C. A. Kaufmann, S. S. Schmidt, J.-P. Bäcker, M. Klaus, C. Genzel, and R. Mainz, Acta Mater. **111**, 377 (2016).
[20] R. Mainz, E. S. Sanli, H. Stange, D. Azulay, S. Brunken, D. Greiner, S. Hajaj, M. D. Heinemann, C. A. Kaufmann, M. Klaus, Q. M. Ramasse, H. Rodriguez-Alvarez, A. Weber, I. Balberg, O. Millo, P. A. van Aken, and D. Abou-Ras, Energy Environ. Sci. **9**, 1818 (2016).
[21] H. Rodriguez-Alvarez, N. Barreau, C. A. Kaufmann, A. Weber, M. Klaus, T. Painchaud, H. W. Schock, and R. Mainz, Acta Mater. **61**, 4347 (2013).
[22] F. Couzinié-Devy, E. Cadel, N. Barreau, L. Arzel, and P. Pareige, Appl. Phys. Lett. **99**, 232108 (2011).
[23] J. Kessler, C. Chityuttakan, J. Lu, J. Schöldström, and L. Stolt, Prog. Photovoltaics Res. Appl. **11**, 319 (2003).
[24] D. Thomas, R. Mainz, H. Rodriguez-Alvarez, B. Marsen, D. Abou-Ras, M. Klaus, C. Genzel, and H. W. Schock, Thin Solid Films **519**, 7193 (2011).
[25] H. Rodriguez-Alvarez, R. Mainz, B. Marsen, and H.-W. Schock, J. Solid State Chem. **183**, 803 (2010).
[26] S. J. Dillon and M. P. Harmer, Mater. Sci. Forum **558–559**, 1227 (2007).
[27] P. L. Chen and I. W. Chen, J. Am. Ceram. Soc. **79**, 1801 (1996).
[28] D. Gupta and P. S. Ho, *Diffusion Phenomena in Thin Films and Microelectronic Materials*, (Noyes Publications, New Jersey, 1989).
[29] Y. Wada and S. Nishimatsu, J. Electrochem. Soc. **125**, 1499 (1978).
[30] S. J. Pennycook and P. D. Nellist, *Scanning Transmission Electron Microscopy: Imaging and Analysis* (Springer, New York, 2011), pp. 1–90.
[31] G. Kresse and J. Furthmüller, Phys. Rev. B **54**, 11169 (1996).
[32] H. Stange, S. Brunken, D. Greiner, M.-D. Heinemann, D. A. Barragan Yani, L. A. Wägele, C. Li, E. Simsek Sanli, M. Kahnt, S. S. Schmidt, J.-P. Bäcker, C. A. Kaufmann, M. Klaus, R. Scheer, C. Genzel, and R. Mainz, J. Appl. Phys. **125**, 035303 (2019).
[33] C. Li, E. S. Sanli, H. Strange, M.-D. Heinemann, D. G. Schäfer, R. Mainz, W. Sigle, D. Abou-Ras, and P. A. van Aken, Microscopy Microanal. **24**, 1492 (2018).
[34] E. S. Sanli, Q. M. Ramasse, W. Sigle, D. Abou-Ras, R. Mainz, A. Weber, H. J. Kleebe, and P. A. van Aken, J. Appl. Phys. **120**, 205301 (2016).
[35] D. Abou-Ras, B. Schaffer, M. Schaffer, S. S. Schmidt, R. Caballero, and T. Unold, Phys. Rev. Lett. **108**, 075502 (2012).
[36] C. Li, J. Poplawsky, Y. Yan, and S. J. Pennycook, Mater. Sci. Semicond. Process. **65**, 64 (2017).
[37] C. Li, Y. Wu, J. Poplawsky, T. J. Pennycook, N. Paudel, W. Yin, S. J. Haigh, M. P. Oxley, A. R. Lupini, M. Al-Jassim, S. J. Pennycook, and Y. Yan, Phys. Rev. Lett. **112**, 156103 (2014).
[38] H. Liu, X. Shi, F. Xu, L. Zhang, W. Zhang, L. Chen, Q. Li, C. Uher, T. Day, and G. S. Jeffrey, Nat. Mater. **11**, 422 (2012).
[39] S. L. White, P. Banerjee, and P. K. Jain, Nat. Commun. **8**, 14514 (2017).

[40] R. Klenk, T. Walter, H. W. Schock, and D. Cahen, Adv. Mater. **5**, 114 (1993).
[41] T. Wada, N. Kohara, T. Negami, and M. Nishitani, J. Mater. Res. **12**, 1456 (1997).
[42] E. S. Sanli, Q. M. Ramasse, R. Mainz, A. Weber, D. Abou-Ras, W. Sigle, and P. A. van Aken, Appl. Phys. Lett. **111**, 032103 (2017).
[43] M. Mock and K. Albe, J. Nucl. Mater. **494**, 157 (2017).